Neuropsychopharmacology

ARTICLE

# Activation of proprotein convertase in the mouse habenula causes depressive-like behaviors through remodeling of extracellular matrix

Hikaru Ito[1,2], Kanako Nozaki[1,3], Kenji Sakimura[4], Manabu Abe[4], Shigeto Yamawaki[5] and Hidenori Aizawa[1]

The lateral habenula (LHb) attracts a growing interest as a regulator of monoaminergic activity which were frequently reported to be defective in depression. Here we found that chronic social defeat stress (CSDS) increased production of pro-inflammatory cytokines in LHb associated with mobilization of monocytes and remodeling of extracellular matrix by increased matrix metalloproteinase (MMP) activity. RNA-seq analysis identified proprotein convertase *Pcsk5* as an upstream regulator of MMP activation, with upregulation in LHb neurons of mice with susceptibility to CSDS. PCSK5 facilitated motility of microglia in vitro by converting inactive pro-MMP14 and pro-MMP2 to their active forms, highlighting its role in mobilization of microglia and monocytes in neuroinflammation. Suppression of *Pcsk5* expression via small interfering RNA (siRNA) ameliorated depressive-like behaviors and pathological mobilization of monocytes in mice with susceptibility to CSDS. PCSK5-MMPs signaling pathway could be a target for development of the antidepressants targeting the inflammatory response in specific brain regions implicated in depression.

*Neuropsychopharmacology* (2021) 46:442–454; https://doi.org/10.1038/s41386-020-00843-0

## INTRODUCTION

Major depression is a pervasive disorder and a leading cause of disability worldwide. Growing evidence supports the view that inflammatory responses in the brain partly underlie the pathophysiology of this disorder [1, 2]. Although monoamines are known to play a critical role in depression, studies have reported that excessive release of pro-inflammatory cytokines alter the synaptic availability of monoamines, which is thought to be an essential mechanism in the pathology of depression [3]. Indeed, previous studies have shown that patients with depression exhibit elevated pro-inflammatory cytokines and chemokines in peripheral blood and cerebrospinal fluid [4]. Despite substantial evidence supporting the involvement of neuroinflammation in depression, the neural substrates which mediate such responses in the context of depressive symptoms remain unclear.

The lateral habenula (LHb) has attracted a surge of interest as a brain region modulating the activity of monoamines such as serotonin and dopamine [5]. Imaging studies have consistently reported altered responses in the habenular region of depressive patients [6, 7], while animal studies have provided consistent evidence that increased activity in the LHb caused depressive-like phenotypes in despair- and conflict-based behavioral paradigms under stress [8–10]. Deep brain stimulation targeting the habenular pathway ameliorated symptoms in a patient with treatment-resistant depression, supporting a role for the habenula in depression [11]. Analyses to date indicate the pivotal role of the habenula in depression, but the molecular and cellular mechanisms underlying how stress affects the habenula to promote depressive-like phenotypes remain unclear. Since studies also reported that acute and chronic stress increased LHb activity with enhanced miniature excitatory postsynaptic current [8] and intracellular calcium concentration [12], exposure of the animal to the persistent stress might modify the long-lasting changes of the cellular and extracellular environment to cause hyperactivation of LHb.

Chronic social defeat stress (CSDS) has been used as a rodent model to examine the molecular machinery underlying depressive-like behaviors developed by the exposure of the smaller animal to the larger aggressor repetitively [13]. Interestingly, it is reported that about a half of mice after CSDS exhibited susceptibility to stress with avoidance of the aggressor, while the rest resilient to the stress rather approached the aggressor for exploration [13]. We previous reported that hyperactivation of LHb with suppression of monoaminergic activation in the brain stem led to the increased susceptibility to CSDS [9]. Thus, understanding the mechanism by which the stress modulates the habenular activity could shed light on the pathophysiology in depressive-like behaviors.

Here, we address the molecular and cellular mechanism underlying it by mRNA profiling of the LHb in mice with depressive-like behaviors under CSDS. CSDS induced neuroinflammatory responses in the LHb with an increase in monocyte infiltration, pro-inflammatory cytokine production, and remodeling of the extracellular matrix (ECM). RNA-seq analysis revealed

[1]Department of Neurobiology, Graduate School of Biomedical and Health Sciences, Hiroshima University, 1-2-3 Kasumi, Minami-ku, Hiroshima 734-8553, Japan; [2]Center for Experimental Animals, Tokyo Medical and Dental University, 1-5-45 Yushima, Bunkyo-ku, Tokyo 113-8510, Japan; [3]Division of Neuroanatomy, Department of Neuroscience, Yamaguchi University Graduate School of Medicine, 1-1-1 Minami-Kogushi, Ube 755-8505, Japan; [4]Department of Cellular Neurobiology, Brain Research Institute, Niigata University, 1-757 Asahimachidori, Chuo-ku, Niigata 951-8585, Japan and [5]Brain, Mind and KANSEI Sciences Research Center, Hiroshima University, 1-2-3 Kasumi, Minami-ku, Hiroshima 734-8553, Japan
Correspondence: Hidenori Aizawa (haizawa@hiroshima-u.ac.jp)

Received: 23 March 2020 Revised: 20 July 2020 Accepted: 25 August 2020
Published online: 17 September 2020

that CSDS facilitated production of proprotein convertase subtilisin/kexin type 5 (*Pcsk5*) by LHb neurons, which activated the matrix metalloproteinase (MMP)14-MMP2 pathway to promote ECM remodeling for neuroinflammation. Knockdown of *Pcsk5* ameliorated depressive-like behavior induced by CSDS with recovery from neuroinflammatory changes in the LHb, suggesting a causal relationship between activation of the PCSK5-MMP pathway and depressive-like phenotypes under CSDS.

## METHODS AND MATERIALS

### Ethics statement

This study was performed in strict accordance with the recommendations of the Guide for the Care and Use of Laboratory Animals of the National Institutes of Health and was approved by the Committees on Animal Experiments (A18-42-3) and the biosafety committee for living modified organisms (30-106) of Hiroshima University.

### Animals

Seven-week-old male C57BL/6J mice (CLEA Japan) were used. For in vitro microglial experiments, Iba1-iCre knockin mice [14] and Rosa-EGFP-Rpl10a knockin mice (#022367, Jackson laboratory, USA) were used to visualize microglia. All mice were kept under a 12-h light-dark cycle at 22–25 °C.

### Chronic social defeat stress

CSDS was performed according to the procedure published previously by the other group [15]. Briefly, 7-week-old C57BL/6J male mice were introduced to the home cage of an unfamiliar aggressive ICR resident mouse for 10 min. Then, experimental mice were separated from the unfamiliar aggressor by a divider and housed on one side of the cage over the subsequent 24 h. These procedures were repeated for 10 consecutive days. Nondefeated control mice were housed two per cage on either side of the divider.

### Behavioral tests

*Open field test*. Mice were placed in the center of an open-field space (50 × 50 × 40 cm) and allowed to explore for 10 min. Light intensity was 5 lux in the center of the field.

*Social avoidance test*. This test was performed as described previously [9]. Briefly, exploratory behavior in the arena was analyzed for the first 2.5 min under illumination with intensity of 5 lux in the presence of a wire mesh enclosure with or without an unfamiliar aggressor mouse. The interaction ratio was calculated as (interaction time with unfamiliar aggressor)/(interaction time with empty cage). We identified the susceptible and resilient mice using <1.0 and ≥1.0 of interaction ratio as criteria, respectively.

*Forced swim test*. Mice were placed individually in 2 L glass beakers containing water at 23 °C. The test was performed under 100 lux illumination. Mice were allowed to swim, and behavior was recorded for 6 min.

*Image analysis of behavioral tests*. ImageOF and ImageFZ software (Mouse Phenotype Database; http://www.mouse-phenotype.org/software.html) were used for behavioral analyses.

### RNA-seq analysis

Mice were killed 48 h after CSDS. Brains were removed and coronally sliced with a vibratome (DTK-1500, Dosaka-EM) at 500 µm. Tissue was rapidly punched under the microscope (MVX10, Olympus) and frozen with liquid nitrogen. Following quality checking of RNA purified using NucleoSpin RNA XS (TAKARA Bio) with the RNA 6000 Pico Kit and 2100 bioanalyzer (Agilent Technologies, Inc.), sequencing libraries (RNA 100 pg) were generated using SMART-Seq v4 Ultra Low Input RNA Kit and Low Input Library Prep Kit v2 (TAKARA Bio) and validated with the Agilent 2100 bioanalyzer. Equal amounts of 12 indexed sequencing libraries were pooled and sequenced on an illumina platform (Hiseq 2500, Illumina Inc.). RNA-seq data are available in the Gene Expression Omnibus under GEO series accession number GSE156965. Sequence reads were mapped against the *Mus musculus* genome assembly (Genome Reference Consortium GRCm38, UCSC mm10) using CLC genomic workbench (QIAGEN). Read count normalization with trimmed mean of *M* values normalization [16], gene expression calculation, and statistical analysis based on generalized linear model were performed by featureCounts [17] and edgeR package [18]. Significance threshold of $p < 0.05$, logCPM > 3, false discovery rate < 0.25, and >1.3-fold change were used.

### RNA extraction and real-time RT-PCR

Total RNA was extracted from brain tissues or primary cultured cells using NucleoSpin RNA XS (TAKARA Bio). Complementary DNA was synthesized using the RiverTra Ace qPCR RT master mix (TOYOBO). Quantitative PCRs were performed with THUNDERBIRD SYBR qPCR Mix (TOYOBO) using a BIO-RAD CFX Connect thermal cycler under the following conditions: 95 °C for 1 min; 50 cycles of 95 °C for 15 s, 60 °C for 30 s, 72 °C for 30 s; and dissociation stage at the last step to verify single amplicons in the reaction. The following primers were used: for Pcsk5, forward 5′-ACTCTTCA GAGGGTGGCTA-3′ and reverse 5′-GCTGGAACAGTTCTTGAATC-3′; for GAPDH, forward 5′-CATGGCCTTCCGTGTTCCT-3′ and reverse 5′-TGATGTCATCATACTTGGCAGGTT-3′; for beta-actin, and forward 5′-CTGTCCCTGTATGCCTCTG-3′ and reverse 5′-ATGTCACGCACGAT TTCC-3′. Primers for GAPDH and β-actin were used to normalize the expression data. Every sample was run in duplicate.

### Cytokine measurement

The amount of pro-inflammatory cytokines tumor necrosis factor-α (TNF-α), interleukin (IL)-1β, and IL-6 in the LHb was measured using beads-based multiplex system (Bio-Plex 200 array, Bio-Rad) according to the manufacturer's instructions. Mice were killed and perfused with ice-cold 0.1 M phosphate-buffered saline (PBS) containing 0.01 M EDTA. Brains were removed and sliced with a vibratome at 500 µm. Tissues were then rapidly punched under a microscope, frozen with liquid nitrogen, and kept at −80 °C until measurement. Samples received five freeze-thaw cycles in TNE buffer (10 mM Tris-HCl, pH 7.8, 10% NP-40, 0.15 M NaCl, and 1 mM EDTA) containing protease inhibitors (protease inhibitor cocktail; Sigma) with liquid nitrogen and sonicated on ice using Bioruptor (UCD-300; Cosmo Bio). Protein concentration was measured with bicinchoninic acid protein assay (MXL-2910, MIXELL, Japan). A total of 25–50 µg protein (1–2 µg/µL) for each sample was mixed with mouse high sensitivity magnetic beads (MHSTCMAG-70K, Merck Millipore, USA) for Bio-Plex assay.

### Histology

Immunohistochemistry was performed as described previously [9] using the following antibodies: rabbit anti-PCSK5 (1:500-1000, ab39873, abcam), mouse anti-NeuN (1:500, MAB377, Millipore), mouse anti-MAP2 antibody (1:2000, sc-32791, Santa Cruz Biotechnology), rabbit anti-Iba1 (1:1000, #013-26471, Wako), rat anti-CD45 (1:500, MCA1388, BioRad), and rabbit anti-S100A9 (1:1000, #73425, Cell Signaling Technology). Signals were visualized with AlexaFluor 488- or 594-conjugated anti-IgGs (Jackson ImmunoResearch Laboratories, Inc.). Sections were counterstained with DAPI. Images were obtained using a confocal microscope (FV-1000D, Olympus).

### Western blotting

Cells were lysed in 62.5 mM Tris-HCl (pH 6.8), 2% (w/v) sodium dodecyl sulfate (SDS), 2.5% (v/v) 2-mercaptoethanol, 5% (v/v)

glycerin, and 0.0025% (w/v) bromophenol blue, and denatured at 95 °C for 5 min. Samples were resolved by 10% SDS-PAGE gels, transferred onto polyvinylidene fluoride (PVDF) membranes (Millipore) and incubated with appropriate antibodies as described below. The membranes were incubated with each primary antibody overnight at 4 °C. Horseradish peroxidase (HRP)-conjugated secondary antibody was added for 2 h at room temperature. Antibody binding was visualized using the ECL Plus Western Blotting reagents (Thermo Fisher Scientific). Mouse anti-MMP2 (1:500, sc-53630, Santa Cruz Biotechnology), mouse anti-MMP9 (1:500, #819701, BioLegend), rabbit anti-MMP14 (1:1000, ab51074, abcam), mouse anti-GAPDH (1:5000, #016-25523, WAKO), and rabbit anti-PCSK5 (1:1000, ab39873, abcam) antibodies were used. Immunoblotted bands were quantified using the ImageJ software after chemiluminescence scanning by myECL Imager (Thermo Fisher Scientific).

### In situ zymography

In situ zymography is an assay for gelatinolytic activity in which cells or tissues are exposed to gelatin as a substrate of MMP2 and MMP9 [19]. Briefly, the sections were cut at 20 µm using freezing microtome and fixed by ethanol for 5 min. Following washes in 0.1 M PBS, the sections were overlaid with a fluorogenic substrate DQ gelatin (1:100, Invitrogen) in the buffer supplied by the manufacturer, and incubated for 40 min at 37 °C. Then, sections were washed with PBS and fixed in 4% PFA for 15 min at room temperature. Sections were counterstained with 4′ 6-diamidino-2-phenylindole (DAPI) and mounted for microscopy. Images were obtained with an inverted fluorescent microscope (ECLIPSE T*i*-U, Nikon). Signal intensities were collected from at least four different slides for each mouse using NIS-elements software (BR3.2, Nikon). To exclude background fluorescence, we used the mean fluorescent intensity of four randomly selected areas between nuclei stained with DAPI as the background signal and subtracted it from fluorescence signals in the LHb on the same slide. The average of the signal intensities was calculated for each mouse, and then the mean values from multiple mice ($N = 3$ or 4) were statistically analyzed between groups.

### Primary microglial and astroglial culture

Primary microglial cultures were prepared according to the procedure published previously by the other group [20]. For astroglial culture, after 10–14 days in culture, the flasks were shaken by hand for 30 min to remove less adherent neurons and microglia. Then, adherent astroglial cells were trypsinized and plated into 6-well cell culture plates ($1 \times 10^5$ cells/well).

### Lipopolysaccharide stimulation for primary microglia

Primary microglia were seeded at 50,000 cells/well into 12-well plate and cultured for 24 h. Cells were treated with or without recombinant human PCSK5 protein (0.01 µg/mL, Abnova) and stimulated with or without Lipopolysaccharide (LPS; 1 µg/mL, SIGMA). After 24 h, cell lysates were collected with lysis buffer (62.5 mM Tris-HCl (pH 6.8), 2% (w/v) sodium dodecyl sulfate (SDS), 2.5% (v/v) 2-mercaptoethanol, 5% (v/v) glycerin, and 0.0025% (w/v) bromophenol blue) for western blotting.

### Primary neuronal culture

Primary cultured neurons were prepared from whole brains of C57BL/6J mice at embryonic day 15 as described previously [21]. For real-time PCR and immunocytochemistry, primary neurons at 5 day in vitro were used.

### Microglial migration assay

Microglial migration was evaluated in vitro using Radius 24-well cell migration assay kit (Cell Biolabs, San Diego, CA) consisting of a circular biocompatible gel in each well according to the manufacturer's instructions. Briefly, microglia were seeded at 20,000 cells/well and cultured for 24 h. Then, the biocompatible gels were removed, and cells were incubated in fresh culture medium with or without recombinant human PCSK5 protein (0.01 µg/mL, Abnova). Cells were allowed to migrate for 4 d. Areas of migrated cells were analyzed with ImageJ software.

### Microglial transmigration assay

Microglial transmigration was evaluated using Transwell inserts (Corning) with a pore size sufficient to permit cell migration. Primary microglia were seeded at 50,000 cells/well on the upper side of a Transwell insert, which bore an uncoated filter with 5.0-µm holes. Seeded Transwell inserts were placed into 24-well plates. The volumes of culture medium were 0.4 and 1.0 mL in the upper and lower chambers, respectively. The microglial cultures were maintained for 1 h. The Transwell inserts containing microglial cells were replaced into new wells with fresh medium with or without recombinant human PCSK5 protein (0.01 µg/mL, Abnova) and incubated for 24 h. Cells remaining on the upper surface of the membrane were removed with cotton-tipped swabs. Following two rinses with 0.1 M PBS, cells were fixed with 4% PFA in 0.1 M PBS and counterstained with DAPI. The number of microglia that had migrated to the underside was counted (five randomly selected fields per membrane). Experiments were performed in triplicate.

### Knockdown by small interfering RNA

We used three candidate small interfering RNA (siRNA) targeting murine Pcsk5: Pcsk5-siRNA #1 (s71338, Thermo Fisher Scientific), Pcsk5-siRNA #2 (s71339, Thermo Fisher Scientific), Pcsk5-siRNA #3 (s71340, Thermo Fisher Scientific), and Control siRNA (Ambion Silencer Negative Control #1 siRNA, #4390843, Thermo Fisher Scientific). Primary cultured neurons were treated with siRNAs using Lipofectamine RNAiMAX transfection reagent (Thermo Fisher Scientific). Forty-eight h later, cells were harvested for real-time PCR. siRNAs were injected into the lateral ventricles of C57BL/6 J adult mice or P1 pups with in vivo-jet PEI transfection reagent (Polyplus Transfection Inc., USA) according to the manufacturer's instructions. Forty-eight hours later, brains were removed and homogenized to extract RNA or proteins for real-time PCR or western blotting as described above.

### Statistical analysis

For two groups, a two-tailed Student's and Welch's *t*-test was used for the data with and without statistical significance by *F*-test, respectively ($p < 0.05$). For comparison of multiple groups, Tukey's HSD or Dunnett test was performed following one-way ANOVA. Statistical significance was defined as a $p$-value < 0.05.

## RESULTS

### CSDS caused mobilization of monocytes with ECM remodeling in the LHb

We hypothesized that alterations in the extracellular microenvironment mediated hyperactivation of the LHb, which in turn led to depressive-like behaviors under chronic stress. To address the neuromodulatory effects of the extracellular microenvironment, we performed quantitative analyses of pro-inflammatory cytokine level using beads-based multiplex assay in the LHb of mice exhibiting increased avoidance behaviors with susceptibility to CSDS (Supplementary Fig. 1a) [13]. Pro-inflammatory TNF-α, IL-1β, and IL-6 measured in the LHb of mice with depressive-like phenotypes with susceptibility to the chronic stress were significantly increased compared to those in nondefeated control mice (Fig. 1a–c). Bone marrow-derived monocytes are recruited to specific brain regions implicated in anxiety responses upon exposure to repetitive social stress where they release pro-inflammatory cytokines [22]. We thus examined the expression of CD45 and S100A9, markers for monocytic lineages [23, 24]. In

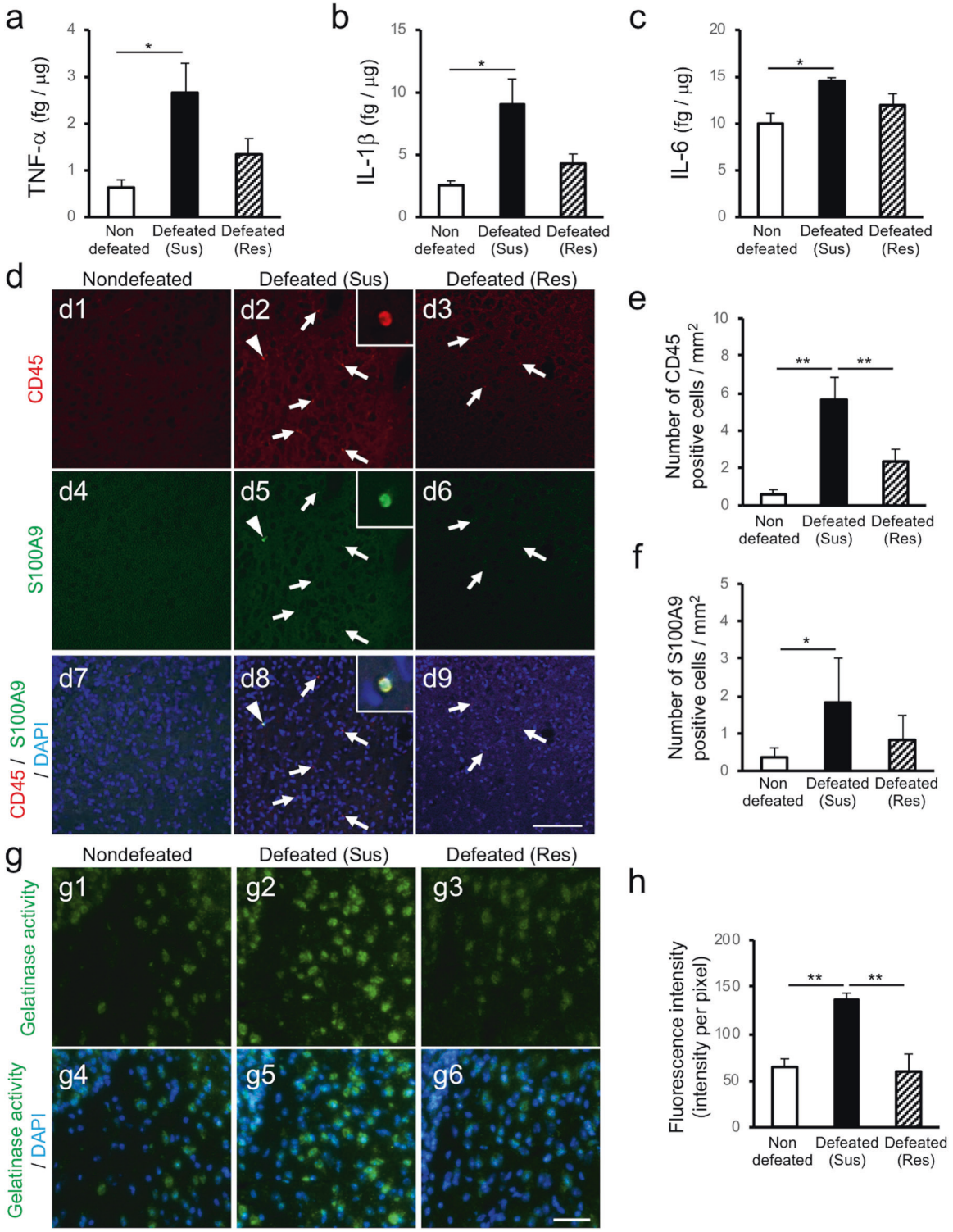


association with increased cytokine production, we observed a larger number of activated monocytes expressing CD45 (red in Fig. 1d, e) and S100A9 (green in Fig. 1d, f) in the LHb of mice susceptible to the defeat stress than in those of nondefeated mice. This was not attributable to changes in the number of microglia, as we did not observe a significant increase in any of the number of cells expressing the pan-microglial marker Iba1 and its expression level (Supplementary Fig. 1b–d).

Rearrangement of the ECM permits recruitment of inflammatory cells [25, 26]. Gelatinases, which consist of MMP2 and MMP9, degrade the ECM and facilitate cell migration for neuroinflammation [27–29]. To investigate the mechanisms underlying the recruitment of monocytes in the LHb, we investigated gelatinase activity by in situ fluorescent zymography [19] (Fig. 1g). Quantitative analysis revealed that the LHb in mice susceptible to CSDS showed greater fluorescence intensity released from quenching gelatin as a substrate for gelatinase compared to that in nondefeated mice (Fig. 1h). These results suggested that depressive-like phenotypes may be related to increased enzymatic activity of gelatinases in the LHb.

**Fig. 1 CSDS triggered the inflammatory responses with microglial mobilization in the LHb. a–c** Bar graphs showing the amount of TNFα [**a**, $p = 0.033$, $F_{2,8} = 6.31$ with one-way ANOVA, $p = 0.030$ (nondefeated vs susceptible), $p = 0.490$ (nondefeated vs resilient), $p = 0.134$ (susceptible vs resilient) with Tukey HSD *post hoc* test], IL-1β [**b**, $p = 0.026$, $F_{2,8} = 7.09$ with one-way ANOVA, $p = 0.025$ (nondefeated vs susceptible), $p = 0.620$ (nondefeated vs resilient), $p = 0.083$ (susceptible vs resilient) with Tukey HSD *post hoc* test] and IL-6 proteins [**c**, $p = 0.037$, $F_{2,8} = 5.98$ with one-way ANOVA, $p = 0.032$ (nondefeated vs susceptible), $p = 0.368$ (nondefeated vs resilient), $p = 0.200$ (susceptible vs resilient) with Tukey HSD *post hoc* test] in the LHb of nondefeated (white), defeated mice with susceptible phenotype (black) and defeated mice with resilient phenotype (hatched) ($N = 3$ for each group). **d** Representative images of the coronal section of the LHb of nondefeated (**d1**, **d4**, **d7**), defeated susceptible mice (**d2**, **d5**, **d8**), and defeated resilient mice (**d3**, **d6**, **d9**) showing CD45-positive (red) and S100A9-positive cells (green). **e** A bar graph showing the number of CD45-positive cells in the LHb of nondefeated (white), defeated susceptible mice (black) and defeated resilient mice (hatched) ($N = 7$ for each group) with statistical contrast ($p = 2.18 \times 10^{-5}$, $F_{2,20} = 20.67$ with one-way ANOVA, $p = 1.57 \times 10^{-5}$ (nondefeated vs susceptible), $p = 0.075$ (nondefeated vs resilient), $p = 0.002$ (susceptible vs resilient) with Tukey HSD *post hoc* test). **f** A bar graph showing the number of S100A9-positive cells in the LHb of nondefeated (white), defeated susceptible mice (black) and defeated resilient mice (hatched) ($N = 5$ for each group) with statistical contrast ($p = 0.028$, $F_{2,14} = 4.86$ with one-way ANOVA, $p = 0.024$ (nondefeated vs susceptible), $p = 0.488$ (nondefeated vs resilient), $p = 0.178$ (susceptible vs resilient) with Tukey HSD *post hoc* test). **g** Representative images of fluorescent *in situ* zymography in the LHb of nondefeated (**g1**, **g4**), defeated mice with susceptibility (**g2**, **g5**) and defeated mice with resilience (**g3**, **g6**) showing green fluorescein released from the gelatin by gelatinase activity (green). **h** A bar graph showing the mean fluorescence intensities per pixel in in situ zymography of the LHb of nondefeated (white, $N = 4$) and defeated mice with susceptibility (black, $N = 5$) and defeated mice with resilience (hatched, $N = 3$) [$p = 0.96 \times 10^{-3}$, $F_{2,20} = 16.58$ with one-way ANOVA, $p = 0.002$ (nondefeated vs susceptible), $p = 0.955$ (nondefeated vs resilient), $p = 0.003$ (susceptible vs resilient) with Tukey HSD *post hoc* test]. Sections were counterstained with DAPI (blue). Values represents mean ± SEM. $^*p < 0.05$; $^{**}p < 0.01$. Scale bars indicated 100 and 50 μm in **d** and **g**, respectively.

Collectively, these findings indicated that exposure to chronic stress promoted recruitment of monocytes to the LHb to release pro-inflammatory cytokines via activation of ECM-degrading proteinase(s). Intriguingly, those changes were not observed in the mice with resilient to CSDS (dashed bars in Fig. 1a–c, e, f, h, d3, d6, d9, g3, g6), suggesting that induction of depressive-like phenotype were associated with neuroinflammatory response of LHb.

## RNA expression profiling revealed increased expression of Pcsk5 in LHb neurons

Members of the MMP family are released from neurons and glia in an inactive form and are activated upon cleavage by other enzymes [28, 30]. To gain insight into the molecular mechanisms underlying activation of ECM-degrading proteinases in the LHb of depressive-like animals, we performed quantitative expression analysis of the genes expressed in the LHb of nondefeated, stress-susceptible, and stress-resilient mice using RNA-seq (Fig. 2a). In addition to the nondefeated mouse group as a control, mice after CSDS were divided into two groups exhibiting high and low susceptibility with regard to social avoidance behavior in the presence of an aggressor mouse as reported previously ($N = 4$ per group, data available in Supplementary Data) [13].

We first checked a specificity of mRNA library collected from LHb (LHb-mRNA) in comparison with the one from the ventral striatum as control (VS-mRNA) of nondefeated mice. *Brn3a*, a POU domain transcription factor specifically expressed in both medial and lateral habenula [31], exhibited 462.0 times higher expression in the LHb-mRNA than the VS-mRNA, suggesting that LHb-mRNA reflected the gene expression profile in the habenular region. More specifically, Prokineticin receptor 2 (*Prokr2*) reported to be expressed specifically in the LHb [32] showed 28.4 time higher expression in LHb-mRNA than VS-mRNA, while the genes such as tachykinin 1 (precursor of substance P, *Tac1*) [33] and solute carrier family 5 member 7 (*Slc5a7* also known as choline transporter) [34] were much less expressed in LHb-mRNA (fold change of −20.7 and −5.5, respectively). These results provided the evidence that LHb-mRNA provided the gene express profile enriched in LHb.

Upon comparison between nondefeated, stress-susceptible, and -resilient mice, among 17,417 genes examined for profiling, we identified 65 and 97 genes showing significant difference in the susceptible group over the nondefeated control group and resilient group, respectively ($p < 0.05$ and false discovery rate <0.25 in likelihood ratio test; Fig. 2b). To examine the specific genes responsible for depressive-like behaviors with increased susceptibility under chronic defeat stress, we targeted the intersection of the two sets (10 genes) to explore candidates for signaling pathways underlying ECM modification. By specifying the target to genes whose expression was significantly correlated with social interaction ratio as a measure of depressive-like phenotype ($p < 0.05$, Fig. 2b and Supplementary Fig. 2), we detected that *Pcsk5* had increased expression in the LHb by 3.215- and 2.011-fold in the susceptible group over the nondefeated and resilient groups, respectively (Fig. 2c).

Activation of gelatinases (MMP2 and MMP9) requires the conversion of inactive pro-MMPs into their active form by a cascade of proteolytic cleavages (Fig. 2d). Since we did not observe a significant increase in transcription levels of MMP2 and MMP9 per se, we screened the expression of genes acting on the activation of MMP2 or MMP9 by referring to the reactome pathway database for the "Activation of Matrix Metalloprotease". Among the 15 genes upstream of MMPs, we observed that only *Pcsk5* had increased expression in groups with social defeat stress (3.215- and 1.599-fold increase in the susceptible and resilient groups, respectively, over the nondefeated group) (Fig. 2e), highlighting *Pcsk5* as a potential upstream regulator of these signaling pathways in the LHb. Since we did not observe the increased transcription of MMPs and other modulators of MMPs pathway in the current analysis (Fig. 2e), upregulation of *Pcsk5* might exert its function via posttranslational modification of MMPs protein for remodeling of ECM.

Furin-like proprotein convertases including *Pcsk5* are serine proteases implicated in the maturation of precursor proteins into their functionally active forms [35]. It is proposed that the PCSK family proteases are central regulators of the membrane type MMPs (MMP14, 15, and 16) that convert inactive pro-MMPs into their active form by a proteolytic cascade [35–37], implicating a role of *Pcsk5* in ECM remodeling for neuroinflammatory responses.

## Proprotein convertase Pcsk5 was increased in habenular neurons of mice susceptible to chronic stress

Expression of *Pcsk5* mRNA in the LHb was negatively correlated with social avoidance ratio as a measure of susceptibility to chronic defeat stress across groups ($R = -0.707$, $p = 0.010$; Fig. 3a). To address regional and cell-type specificity of this gene, we examined the distribution of *Pcsk5* mRNA and protein expression in the murine brain. Quantitative polymerase chain reaction (PCR) analysis revealed that *Pcsk5* was enriched in the LHb over other brain regions implicated in the susceptibility of animals to chronic stress (Fig. 3b). PCSK5 protein was distributed in epithalamic regions including the medial and lateral habenula as well as paraventricular thalamic nucleus (PVT) (Fig. 3c). The majority of LHb cells expressing PCSK5 protein co-expressed the neuronal marker NeuN, suggesting neurons as a primary source of PCSK5

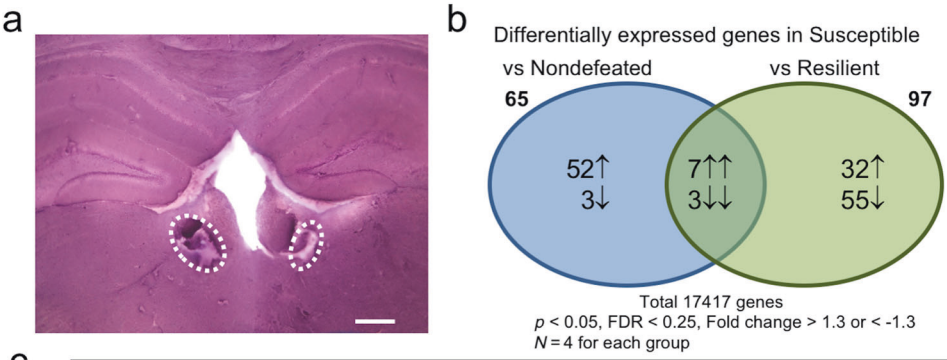


c

| Gene Symbol | Fold change: Susceptible vs Nondefeated | Fold change: Susceptible vs Resilient | Fold change: Resilient vs Nondefeated | Likelihood ratio test: p value | Likelihood ratio test: FDR | Pearson's correlation coefficient: Correlation coefficient (R) | Pearson's correlation coefficient: p value |
|---|---|---|---|---|---|---|---|
| *Pcsk5* | 3.215 | 2.011 | 1.599 | 0.001 | 0.164 | -0.707 | 0.010 |
| *Kat6a* | -2.365 | -1.416 | -1.670 | 0.001 | 0.164 | 0.587 | 0.045 |
| *Usp31* | -2.413 | -1.632 | -1.479 | 0.002 | 0.209 | 0.738 | 0.006 |
| *Etv6* | -4.284 | -4.065 | -1.054 | 0.002 | 0.209 | 0.659 | 0.020 |

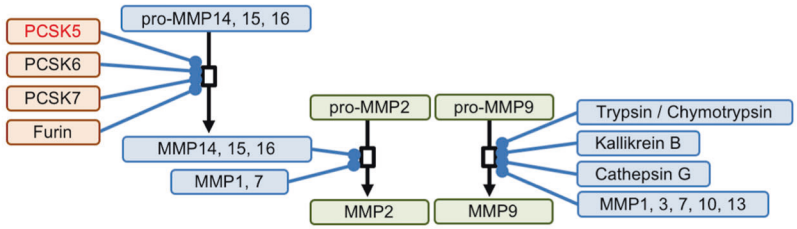


e

| Gene Symbol | Fold change: Susceptible vs Nondefeated | Fold change: Susceptible vs Resilient | Fold change: Resilient vs Nondefeated | p value |
|---|---|---|---|---|
| *Pcsk5* | 3.215 | 2.011 | 1.599 | 0.001 |
| *Pcsk6* | -1.064 | 1.354 | -1.441 | 0.624 |
| *Pcsk7* | -1.314 | 1.181 | -1.552 | 0.247 |
| *Furin* | -1.632 | 1.048 | -1.709 | 0.220 |
| *Mmp14* | 1.065 | -1.255 | 1.336 | 0.592 |
| *Mmp15* | -1.040 | 1.079 | -1.122 | 0.937 |
| *Mmp16* | -1.293 | -1.191 | -1.085 | 0.711 |
| *Mmp2* | 1.597 | 2.297 | -1.438 | 0.616 |

| Gene Symbol | Fold change: Susceptible vs Nondefeated | Fold change: Susceptible vs Resilient | Fold change: Resilient vs Nondefeated | p value |
|---|---|---|---|---|
| *Mmp1* | ND | NA | ND | NA |
| *Mmp3* | ND | NA | ND | NA |
| *Mmp7* | ND | NA | ND | NA |
| *Mmp10* | ND | NA | ND | NA |
| *Mmp13* | ND | NA | ND | NA |
| *Chymotrypsin C* | ND | NA | ND | NA |
| *Kallikrein B* | ND | NA | ND | NA |
| *Cathepsin G* | ND | NA | ND | NA |
| *Mmp9* | -1.903 | -2.472 | 1.299 | 0.251 |

**Fig. 2 Upregulation of proprotein convertase *Pcsk5* mRNA in the LHb with CSDS. a** Coronal section of the murine epithalamus with hematoxylin and eosin staining showing areas processed for RNA-seq analysis (dashed lines). Scale bar, 100 μm. **b** Venn diagrams showing the intersection of differentially expressed genes in the LHb of defeated mice with susceptibility (Susceptible) versus nondefeated (blue) and Resilient groups (green). **c** Table showing the genes with fold-change in expression of the susceptible group over the nondefeated group and resilient groups. Results of the statistical analyses with *p*-values and false discovery rate (FDR) for three group comparison in likelihood ratio test and with *p*-values and correlation coefficient (*R*) in Pearson's correlation analysis are presented. Genes were chosen according to the fold-change between groups > 1.3, $p < 0.05$, logCPM > 3, and FDR < 0.25. **d** Schematic of the signaling pathways for activation of MMP2 (gelatinase A) and MMP9 (gelatinase B) according to the information available on reactome pathway database "Activation of Matrix Metalloprotease". **e** Table showing fold-changes and *p*-values of expression of genes known to activate MMP2 (left) and MMP9 (right) in susceptible and resilient groups over the nondefeated group. ND not detected. NA not available.

production in the LHb (Fig. 3d). This view was supported by in vitro analysis in which primary culture cells enriched in neurons using whole embryonic brains exhibited higher expression levels of *Pcsk5* mRNA than those enriched in astrocytes or microglia (Fig. 3e). Indeed, primary culture neurons expressing neuronal marker MAP2 extended multiple neurites, corroborating the neuronal expression of PCSK5 (Fig. 3f). Although *Pcsk5* consists of two isoforms that share a catalytic domain, RNA-seq analysis revealed a predominance of shorter *Pcsk5a* expression, suggesting that *Pcsk5a* may play a more important role in the LHb (Supplementary Fig. 3a, b).

Quantitative PCR analysis revealed that *Pcsk5a* (hereafter *Pcsk5*) expression in LHb was significantly higher in susceptible but not resilient mice after CSDS than nondefeated control (Supplementary Fig. 3c, left). This upregulation of *Pcsk5* in response to the chronic stress was peculiar to LHb, since we did not observe such an effect in PVT adjacent to the LHb (Supplementary Fig. 3c, right).

These results collectively indicated that LHb neurons were a source of increased *Pcsk5* in mice susceptible to chronic defeat stress.

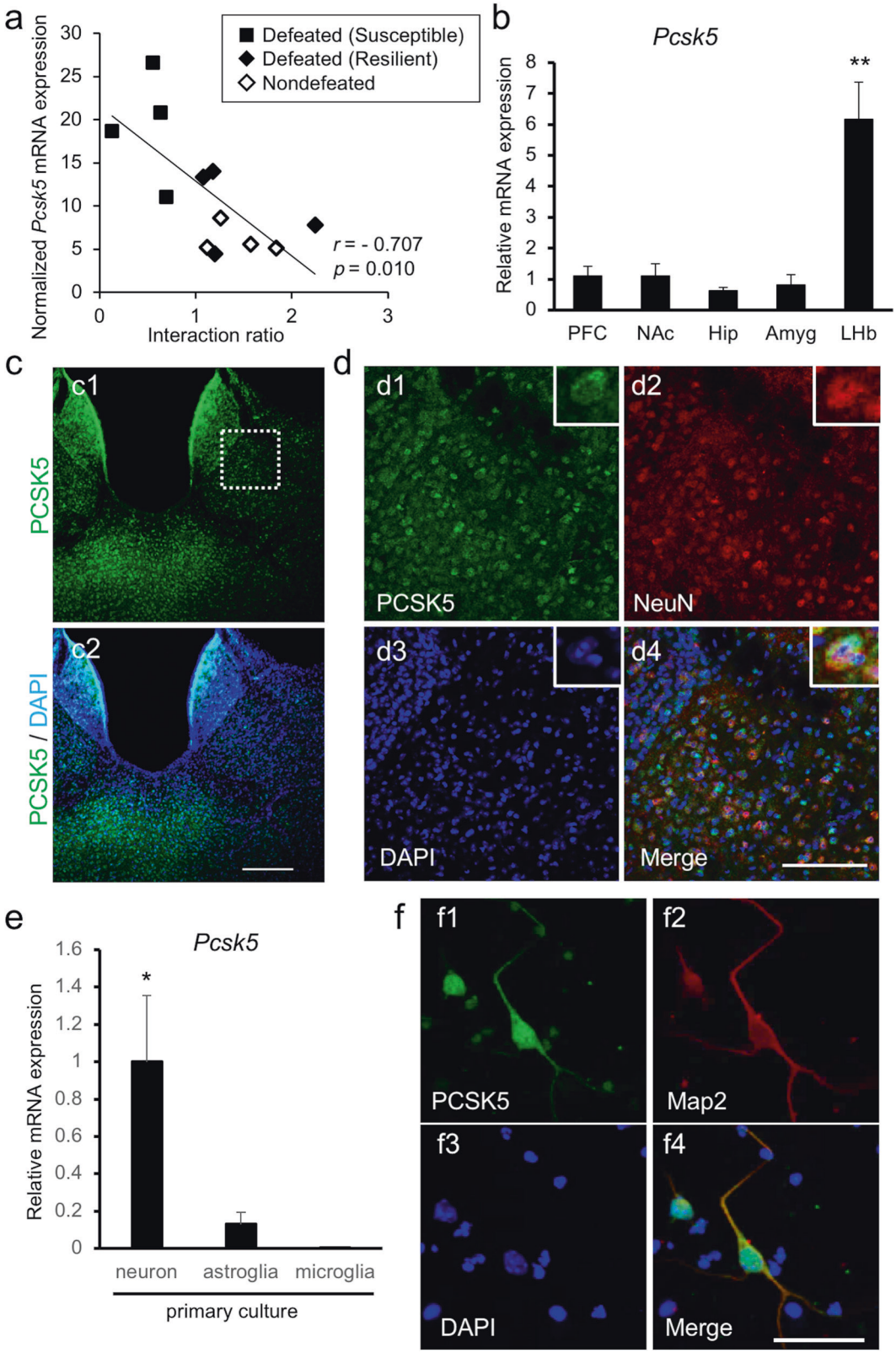


PCSK5 enhanced cell migration through activation of MMP14-MMP2 signaling

To examine the molecular mechanisms underlying increased PCSK5, we investigated the activation of MMPs in vitro. Previous studies reported that MMP14 (also known as membrane type-MMP1) converts inactive pro-MMP2 into active MMP2 by endoproteolytic cleavage [38, 39]. As PCSK5 activates MMP14 by converting inactive pro-MMP14 to its active form in macrophages in atherosclerotic plaques [40], we hypothesized that PCSK5 would facilitate cell motility by activating MMP14-MMP2 cascade signaling.

**Fig. 3 CSDS caused upregulation of Pcsk5 expression in LHb neurons. a** Graph showing negative correlation between *Pcsk5* mRNA expression and interaction ratio in the social avoidance test across groups including nondefeated (open rhombus), defeated mice with susceptibility (filled rectangle), and resilient mice (filled rhombus) ($R = -0.707$, $p = 0.010$, Pearson's correlation). Normalized *Pcsk5* mRNA expression was calculated from raw read counts of RNA-seq data. **b** Bar graph of *Pcsk5* mRNA expression in the prefrontal cortex (PFC), nucleus accumbens (NAc), hippocampus (Hip), amygdala (Amyg), and LHb by quantitative PCR showing statistical comparison of the LHb over PFC ($p = 0.0002$ with Tukey HSD post hoc test), NAc ($p = 0.0002$), Hip ($p = 9.46 \times 10^{-5}$), and Amyg ($p = 0.0001$; $N = 4$, $p = 3.92 \times 10^{-5}$, $F_{4,19} = 15.06$ in one-way ANOVA). **c** Coronal section of the mouse habenula showing expression of PCSK5 (green) and nuclear staining (DAPI, blue). **d** High magnification of a coronal section of the mouse LHb showing the expression of PCSK5 (green), NeuN (red), and nuclear staining (DAPI, blue). **e** Bar graph of *Pcsk5* mRNA expression in primary cultured cells (neurons, astroglia, and microglia) ($N = 4$, $p = 0.015$, $F_{2,11} = 6.87$ in one-way ANOVA; $p = 0.038$ and 0.019 for neurons versus astroglia and neurons versus microglia with Tukey HSD post hoc test, respectively). **f** Images showing the expression of PCSK5 (green, **f1**), MAP2 (red, **f2**), and nuclear staining (DAPI, blue, **f3**) in primary cultured neurons. Values are presented as mean ± SEM. $*p < 0.05$; $**p < 0.01$. Scale bars indicate 100, 50, and 20 μm in **c**, **d**, and **f**, respectively.

To assess whether PCSK5 activated MMP2 via conversion of pro-MMP14 by its proteinase activity, we performed western blotting analysis. Analysis of proteins from primary microglial culture cells known to express MMPs [41, 42] revealed that the proportion of MMP14 relative to pro-MMP14 was significantly increased in the presence of recombinant human PCSK5, while the amount of pro-domain in MMP14 was comparable between groups with and without PCSK5 (Fig. 4a, b). Concordant with MMP14 as an upstream regulator of PCSK5 resulting in conversion of pro-MMP2 to active MMP2, we observed a larger amount of MMP2 protein in the group treated with PCSK5 than in the group treated with vehicle (Fig. 4c, d). We did not observe the effect of PCSK5 on activation of MMP9, another proteinase with gelatinase activity, while active form MMP9 emerged by LPS stimulation which was previously reported to activate MMP1 and MMP3 acting as upstream regulator of MMP9 activation [43] (Supplementary Fig. 4), suggesting that PCSK5 targeted MMP2 more preferentially than MMP9.

Activated MMPs may enhance cell migration [44–46]. To address the role of activated MMP2 by PCSK5 in the modulation of motility of the mobile cells such as microglia and monocytes, we performed radius gel migration assay in which primary culture microglia migrated along the horizontal plane on a culture dish into a cell-free area at the center (Fig. 4e). Quantitative analysis of the number of cells that migrated into the cell-free area on 0, 2, and 4 days after the onset of treatment revealed that recombinant human PCSK5 significantly increased migration by nearly 2-fold (Fig. 4f, day 2; control: 17.6 ± 1.4% vs. PCSK5 treated: 29.8 ± 5.9%, day 4; control: 38.3 ± 1.8% vs. PCSK5 treated: 63.2 ± 7.9%). We further investigated three-dimensional motility of microglia for transmigration in the Transwell [47, 48]. Cultured microglia placed in the upper chamber of Transwell transmigrated more actively across the membrane within 24 h, revealing a larger number of microglia in the underside of the chamber in the presence of PCSK5 (Fig. 4g, h), implying that PCSK5 enhanced cell migration ability.

### Suppression of Pcsk5 ameliorated depressive behaviors and pathological mobilization of microglia in susceptible mice

As Pcsk5 was upregulated in mice with depressive-like behaviors, we hypothesized that suppression of Pcsk5 function would have antidepressant effects on stress-induced behavioral outcomes. To address this, we screened siRNAs to knockdown murine Pcsk5 using primary cultured neurons. Quantitative PCR analysis indicated that Pcsk5-siRNA #3 significantly decreased *Pcsk5* mRNA expression (Supplementary Fig. 5a). In line with this in vitro result, intracerebroventricular (ICV) injection of Pcsk5-siRNA #3 significantly reduced *Pcsk5* mRNA, which led to reduced PCSK5 protein in the brains of postnatal day 3 pups (Supplementary Fig. 5b, c, d). Based on these observations, we selected Pcsk5-siRNA #3 (hereafter Pcsk5-siRNA) and applied it in in vivo analysis as described below.

We first checked the effect of Pcsk5-siRNA in nondefeated mice in the open field test, social avoidance test and forced swim test 48 h before (Pre-siRNA test) and after siRNA injection (Post-siRNA test; Fig. 5a), since we observed a significant reduction of *Pcsk5* mRNA in the LHb 48 h after ICV injection of Pcsk5-siRNA (Fig. 5b). Histological analysis revealed that ICV injection of Pcsk5-siRNA to the adult mice induced significant reduction of PCSK5 protein both in LHb and PVT (Supplementary Fig. 6). Results showed that none of those tests revealed the Pcsk5-siRNA-specific effect on behaviors (Fig. 5c–e), although ICV injection reduced the total distance in the open field irrespective of the siRNA treatment, possible due to surgical manipulation (Fig. 5c).

To investigate the role of *Pcsk5* in depressive-like behaviors induced by chronic social defeat stress, we examined the effects of *Pcsk5* knockdown in the open field and social avoidance test of mice susceptible to chronic stress. We did not observe significant difference in total distance traveled in the open field in the open field across siRNA treatment and between groups, suggesting that neither chronic stress nor ICV injection altered locomotor activity (Fig. 5f). We observed that mice spent a longer interaction time with the aggressor after Pcsk5-siRNA treatment as shown by higher interaction ratio in post-siRNA than in Pre-siRNA of the Pcsk5-siRNA group (Fig. 5g). Since the interaction ratio after siRNA was significantly higher in the Pcsk5-siRNA group than in the Control-siRNA group, social avoidance behavior impaired by chronic stress was ameliorated by specific targeting of *Pcsk5*. Behavioral changes were unlikely to be due to ICV injection of solution, as Control-siRNA did not significantly change the interaction ratio. In the despair-based behavioral test for antidepressant screening, we observed that Pcsk5-siRNA treatment reduced despair-like behaviors as measured by shorter time spent immobile in the forced swim test (Fig. 5h).

These results suggested that reduction of *Pcsk5* expression in the epithalamic region ameliorated stress-induced depressive-like behaviors in mice.

### Pcsk5 knockdown suppressed inflammatory responses in the habenula via remodeling of the extracellular environment

Following our observations that *Pcsk5* activated the MMP14-MMP2 pathway, we examined gelatinase activity in the LHb of mice susceptible to chronic defeat stress with Control- or Pcsk5-siRNA treatment to explore the cellular mechanisms underlying the amelioration of stress-induced behaviors. In situ zymography revealed that relative to Control-siRNA treatment, Pcsk5-siRNA treatment inhibited stress-induced gelatinolytic activity in the LHb in mice susceptible to chronic stress (Fig. 5I, j). Consistent with the recovery of the extracellular milieu as described above, chronic stress induced smaller numbers of CD45-positive monocytes (Fig. 5k, l) and S100A9-positive activated monocytes (Fig. 5m, n) in the LHb of Pcsk5-siRNA-treated group than in that of the Control-siRNA-treated group. We further investigated whether the suppression of stress-induced mobilization of microglia and monocytes resulted in the reduction of cytokines using a microbeads-based protein assay. Mice susceptible to chronic stress exhibited partially reduced production of pro-inflammatory cytokines such as TNF-α (Fig. 5o), IL-1β (Fig. 5p),

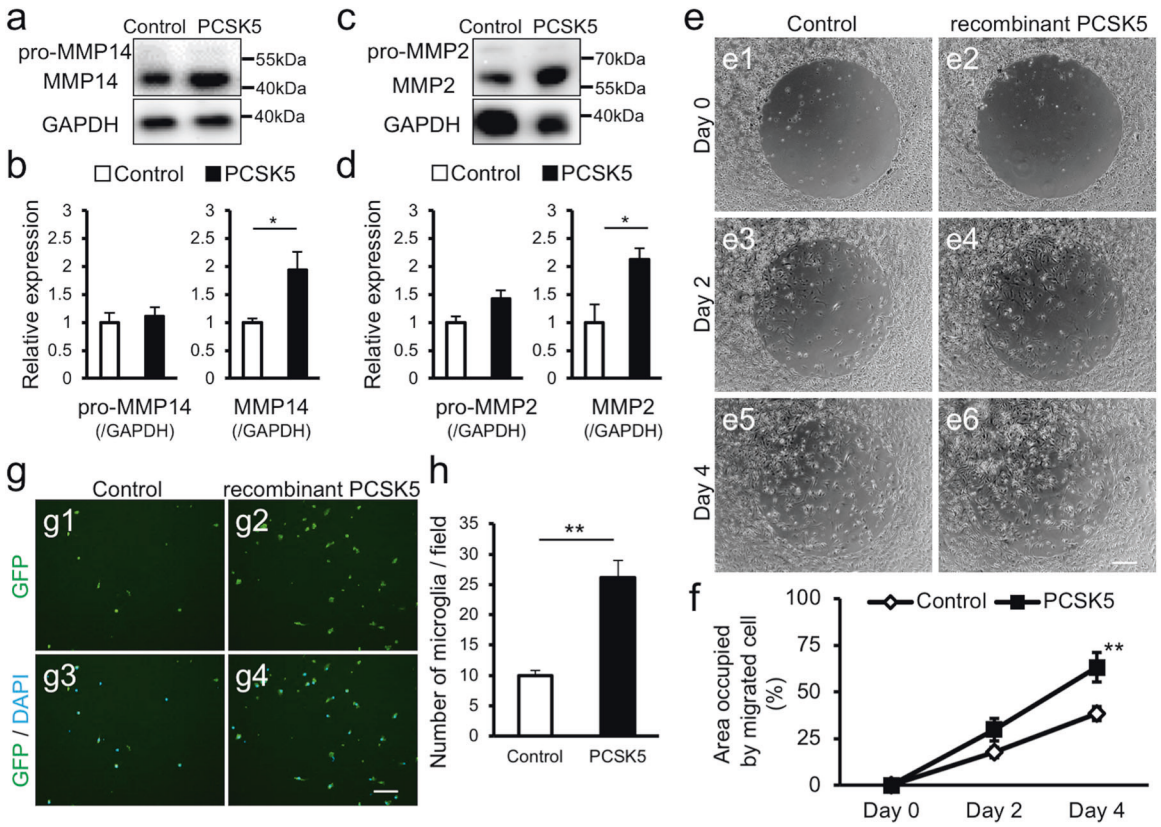


**Fig. 4 PCSK5 facilitated microglial migration via activation of the MMP14-MMP2 signaling pathway. a**, **c** Western blotting of total protein extracted from primary cultured microglia with control and PCSK5 media with anti-MMP14 (**a**) and anti-MMP2 antibodies (**c**) as well as GAPDH antibodies (**a**, **c**). **b**, **d** Bar graphs of the relative expression of pro-MMP14/MMP14 (**b**) and pro-MMP2/MMP2 (**d**) proteins showing a larger amount of mature forms of MMP14 (**b**) and MMP2 (**d**) by PCSK5 (black) than by control (white; $N = 3$ per group; $t_4 = -0.49$, $p = 0.653$ for pro-MMP14; $t_4 = -2.89$, $p = 0.045$ for MMP14; $t_4 = -2.21$, $p = 0.091$ for pro-MMP2; $t_4 = -2.93$, $p = 0.043$ for MMP2). **e** Representative phase contrast images of the radius gel migration assay of the primary microglial culture with vehicle (control; **e1**, **e3**, **e5**) and human recombinant PCSK5 (**e2**, **e4**, **e6**) taken at day 0, 2, and 4 after removing the circular gel at the center of the field. **f** Line plot of the area occupied by microglia migrating into the central area in the radius gel migration assay on days 0, 2, and 4 showing a greater increase in the presence of PCSK5 than in Control ($N = 4$ for each group; $p = 1.26 \times 10^{-8}$, $F_{5,23} = 34.62$ in one-way ANOVA; $p = 0.005$ with Tukey HSD post hoc for control versus PCSK5 treatment on day 4). **g** Representative images of the transmigration assay using primary culture microglia from Iba1-Cre; Rosa-Rpl10a-EGFP mutants on the underside of Transwell chambers showing green fluorescence in cell bodies in the absence (control, **g1** and **g3**) and presence of recombinant PCSK5 protein (**g2** and **g4**). Cell nuclei were stained with DAPI (blue in **g3** and **g4**). **h** Bar graph showing the number of cells in the underside of a Transwell chamber through transmigration per field in control (white) and PCSK5 groups (black) in the transmigration assay. ($N = 3$ for each group, $t_4 = -5.46$, $p = 0.005$). Values indicate mean ± SEM. *$p < 0.05$; **$p < 0.01$. Scale bars, 100 µm.

and IL-6 (Fig. 5q) following knockdown of Pcsk5 by siRNA. These results implied that suppression of Pcsk5 had antidepressant effects and improved pathological changes of the extracellular microenvironment in the LHb of mice after chronic defeat stress.

## DISCUSSION

In the current study, we report for the first time a role of *Pcsk5* in stress-induced depressive-like behaviors in mice via activation of the MMP2 pathway for ECM remodeling. Below, we discuss how chronic stress affects the extracellular milieu in the LHb, which leads to depressive-like behaviors in mice.

### Altered extracellular microenvironment in the LHb leads to depressive-like behaviors

A growing number of studies supported that LHb plays pivotal roles in induction of depressive-like behaviors in rodents via modulation of monoaminergic activity [49]. Indeed, we previously showed that hyperactivation of LHb neurons suppressed the activation of monoaminergic neurons in the brain stem, leading to the exaggeration of despair-like and avoidance behaviors in mice under the stress [9]. More recently, studies supported a role of glia in modulation of LHb neurons showing burst activity in association with depressive-like behaviors [50]. Despite accumulating evidence for roles of LHb in depressive-like behaviors, it remains elusive how the LHb neurons change activity under the stress.

Extracellular microenvironment such as humoral factors and ECM integrity are known as important factors for modulation of neuronal excitability [30, 51, 52]. Recent studies revealed that activation of MMPs triggers a variety of inflammatory responses in the extracellular space [25, 39]. Although it triggers impairment the BBB permeability and mobilization of inflammatory cells such as microglia and monocytes in CNS [28], molecular mechanism underlying interplay between neurons and ECM under the environmental challenge such as social stress. Our results showing roles of Pcsk5 released from the LHb neurons in remodeling of ECM via MMP activation provided a novel pathway leading neuronal activity to modulate extracellular microenvironment for mobilization and infiltration of immune and glial cells (Supplementary Fig. 7).

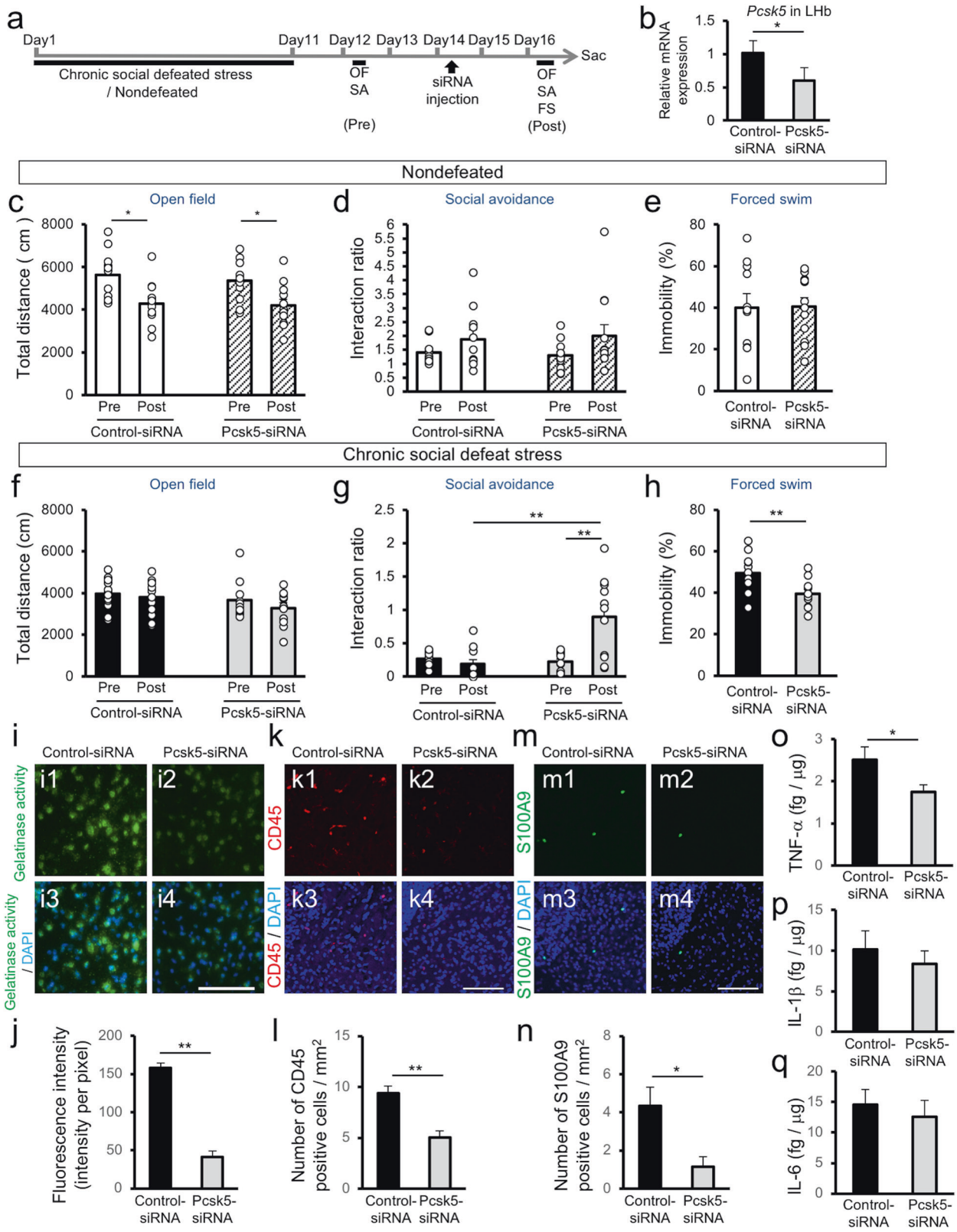


Proprotein convertase triggers neuroinflammatory responses via activation of MMP pathways

MMP-2 and MMP-9 constitute one of the major subclasses of the MMP family with gelatinase activity [28, 30]. In support of neuroinflammatory responses in depression, these MMPs have been implicated in its pathophysiology. For example, serum MMP2 was increased [53], while MMP9 was decreased in depressive patients after a course of electroconvulsive therapy [54].

PCSK5 belongs to the proprotein convertase family and activates precursor proteins by cleavage at specific sites [35].

**Fig. 5 Knockdown of *Pcsk5* ameliorated stress-induced depressive-like behaviors by suppressing mobilization of activated microglia in the LHb. a** Schedule for behavioral tests after CSDS in mice treated with control or Pcsk5-siRNA. OF: Open field test, SA social avoidance test, FS forced swim test. **b** Bar graph of *Pcsk5* mRNA expression in the LHb 48 h after control- (black) and Pcsk5-siRNA injection (gray) showing statistical comparisons indicated by an asterisk ($N = 4$ for each group, $p = 0.021$, $t_6 = 3.11$). **c**–**h** Bar graphs of the total distance traveled in the open field test (**c**, **f**), interaction ratio in the social avoidance test (**d**, **g**) and percentage of time spent in immobile in the forced swim test (**e**, **h**) with injection of control- (white in **c**–**e** for nondefeated group, $N = 11$; black in **f**–**h** for defeated group, $N = 12$) and Pcsk5-siRNA (hashed in **c**–**e** for nondefeated group, $N = 12$; gray in **f**–**h** for defeated group, $N = 11$) 48 h before (Pre) and after (Post) siRNA injection in nondefeated (**c**–**e**, $p = 0.002$, $F_{3,45} = 5.69$ with one-way ANOVA followed by Tukey HSD post hoc test for open field test ($p = 0.021$ and $p = 0.043$ for Pre-control-siRNA vs Post-control-siRNA and Pre-Pcsk5-siRNA vs Post-Pcsk5-siRNA, respectively); $p = 0.231$, $F_{3,45} = 1.49$ with one-way ANOVA for social avoidance test; $p = 0.956$, $t_{21} = -0.06$ with two-tailed Student's *t* test for forced swim test) and defeated mice (**f**–**h**, $p = 0.257$, $F_{3,45} = 1.40$ with one-way ANOVA for open field test; $p = 7.56 \times 10^{-6}$, $F_{3,45} = 12.12$ with one-way ANOVA followed by Tukey HSD post hoc test for social avoidance test ($p = 7.63 \times 10^{-5}$ and $p = 2.85 \times 10^{-5}$ for Pre-Pcsk5-siRNA vs Post-Pcsk5-siRNA and Post-Control-siRNA vs Post-Pcsk5-siRNA, respectively); $p = 0.008$, $t_{21} = 2.96$ with two-tailed Student's *t* test for forced swim test). **i** Representative images of fluorescent in situ zymography of gelatinase activity in the LHb of control- (**i1** and **i3**) and Pcsk5-siRNA injected mice (**i2** and **i4**). **j** Bar graph of the quantified fluorescence intensity per pixel in situ zymography of the LHb with control- (black) and Pcsk5-siRNA group (gray) showing a significant reduction in gelatinase activity after *Pcsk5* knockdown ($N = 4$, $p = 2.42 \times 10^{-5}$, $t_6 = 11.64$ with two-tailed Student's *t* test). **k**, **m** Coronal sections of the LHb treated with control- (**k1**, **k3**, **m1**, **m3**) and Pcsk5-siRNA (**k2**, **k4**, **m2**, **m4**) showing distribution of CD45-positive monocytes/macrophages (red in **k**) and S100A9-positive monocytes/macrophages (green in **m**). **l, n** Bar graphs of the number of CD45-positive cells per field in the LHb of mice with control-siRNA (black, $N = 8$) and Pcsk5-siRNA (gray, $N = 7$; $p = 0.62 \times 10^{-3}$, $t_{13} = 4.48$ and $p = 0.016$, $t_{13} = 2.76$ for CD45- and S100A9-positive cells with two-tailed Student's *t* test, respectively). Sections were counterstained with DAPI (blue in **i**, **k**, **m**). **o–q** Bar graphs showing the amount of TNFα, IL-1β, and IL-6 in the LHb of mice treated with control- (black) and Pcsk5-siRNA (gray; $N = 6$ for each group, $t_{10} = 2.28$, $t_{10} = 0.66$, $p = 0.527$ for IL-1β; $t_{10} = 1.36$, $p = 0.564$ for IL-6). Values are presented as mean ± SEM. $^*p < 0.05$; $^{**}p < 0.01$. Scale bars, 100 μm.

Previous studies reported that predominant PCSK5a were secreted into the extracellular space, while the PCSK5b were kept tethered to the plasma membrane [55, 56], suggesting that upregulation of PCSK5a could act non cell-autonomously on the cells distant to the secreting cells. Effect of PCSK5 converting inactive MMP14 and MMP2 to the active forms on cell motility as shown in the current study implied that the ECM remodeling via activation of PCSK5-MMPs pathway might facilitate the mobilization of monocytes in LHb of mice after chronic stress.

Although proprotein convertases have been implicated in tumor progression and metastasis through the activation of their substrates such as MMP2 and MMP9 [35, 57], few studies have addressed their roles in animal behaviors. Our results identified a role for Pcsk5 in activating the MMP14-MMP2 pathway associated with neuroinflammatory responses in a mouse model useful to study depression, suggesting that a neuron-derived secretory factor modulates the ECM microenvironment, which reciprocally affects neuronal activity.

A study previously implicated PCSK5 with depression based on a case with frameshift mutation of PCSK5 without discussing its role in its pathophysiology [58]. Since current study revealed a role of PCSK5-MMPs pathway in cellular mechanism underlying the neuroinflammatory response of the brain to the stress, current study would provide a novel aspect of PCSK5 in depression.

PCSK5-MMP pathway and depressive-like behavior

Current study identified Pcsk5 mRNA whose expression in the LHb neurons was upregulated after chronic stress. Since it is reported that LHb neurons are activated in response to the aversive stimuli and punishment, PCSK5 might facilitate the change in firing pattern of LHb neurons as reported previously [10] via glial activation and ECM remodeling. Taking the LHb-specific increase of Pcsk5 mRNA into consideration as shown in the current study, it is likely that PCSK5-MMP pathway in LHb contributes significantly to the depressive-like phenotype.

However, since we also observed that PCSK5 protein level consistently decreased in PVT as well as LHb by Pcsk5-siRNA as compared to Control-siRNA, we could not exclude a possibility that Pcsk5 reduction in the brain region outside LHb contributed to the antidepressant effect of ICV injection of Pcsk5-siRNA. LHb-specific reduction of *Pcsk5* by conditional knockdown or knockout strategy in combination with region-specific transduction of viral vector would clarify a role of *Pcsk5* in the neural substrate underlying depressive-like behaviors under the stress.

## CONCLUSION

Currently, brain-immune interactions have been discussed as the risk and resilience factors for depression. Despite highlight of anti-inflammatory treatment in depression, plausible molecular target acting on a specific neural pathway are still under investigation. Current study proposes *Pcsk5* as a target of antidepressant development for a subpopulation of depression associated with neuroinflammation.

## FUNDING AND DISCLOSURE

This study was supported by funds from the Kato Memorial Bioscience Foundation; by a Grant-in-Aid for Scientific Research on Innovative Areas (KAKENHI26112010 & JP19H05723) and a Grant-in-Aid for Challenging Exploratory Research (KAKENHI17K19459) from the Ministry of Education, Culture, Sports, Science and Technology (MEXT) to HA and a Grant-in-Aid for 'Integrated Research on Depression, Dementia and Development Disorders (18dm0107093h0003)' carried out under the Strategic Research Program for Brain Sciences by AMED to SY. The authors declare no competing interests.

## ACKNOWLEDGEMENTS

We thank Dr. Deepa Kamath Kasaragod for critical reading of the manuscript and Ms. Yuka Ishimaru, Ms. Sawako Ogata, Ms. Fumie Nishimura, Ms. Saori Okamura, and Natural Science Center for Basic Research and Development of Hiroshima University for the technical assistance. This research was supported by the Program of the Network-type Joint Usage/Research Center for Radiation Disaster Medical Science.

## AUTHOR CONTRIBUTIONS

HI and HA designed the study and wrote the manuscript. HI and KN performed experiments and analyzed data. KS and MA contributed new analytic tools. SY provided intellectual inputs.

## ADDITIONAL INFORMATION

**Supplementary Information** accompanies this paper at (https://doi.org/10.1038/s41386-020-00843-0).

**Publisher's note** Springer Nature remains neutral with regard to jurisdictional claims in published maps and institutional affiliations.

## REFERENCES

1. Miller AH, Raison CL. The role of inflammation in depression: from evolutionary imperative to modern treatment target. Nat Rev Immunol. 2016;16:22–34.
2. Weber MD, Godbout JP, Sheridan JF. Repeated social defeat, neuroinflammation, and behavior: monocytes carry the signal. Neuropsychopharmacology 2017;42:46–61.
3. Duman RS, Aghajanian GK, Sanacora G, Krystal JH. Synaptic plasticity and depression: new insights from stress and rapid-acting antidepressants. Nat Med. 2016;22:238–49.
4. O'Brien SM, Scott LV, Dinan TG. Cytokines: abnormalities in major depression and implications for pharmacological treatment. Hum Psychopharmacol. 2004;19:397–403.
5. Aizawa H, Cui W, Tanaka K, Okamoto H. Hyperactivation of the habenula as a link between depression and sleep disturbance. Front Hum Neurosci. 2013;7:826.
6. Lawson RP, Nord CL, Seymour B, Thomas DL, Dayan P, Pilling S, et al. Disrupted habenula function in major depression. Mol Psychiatry. 2017;22:202–8.
7. Salas R, Baldwin P, de Biasi M, Montague PR. BOLD responses to negative reward prediction errors in human habenula. Front Hum Neurosci. 2010;4:36.
8. Li B, Piriz J, Mirrione M, Chung C, Proulx CD, Schulz D, et al. Synaptic potentiation onto habenula neurons in the learned helplessness model of depression. Nature 2011;470:535–9.
9. Cui W, Mizukami H, Yanagisawa M, Aida T, Nomura M, Isomura Y, et al. Glial dysfunction in the mouse habenula causes depressive-like behaviors and seep disturbance. J Neurosci. 2014;34:16273–85.
10. Yang Y, Cui Y, Sang K, Dong Y, Ni Z, Ma S, et al. Ketamine blocks bursting in the lateral habenula to rapidly relieve depression. Nature 2018;554:317–22.
11. Sartorius A, Kiening KL, Kirsch P, von Gall CC, Haberkorn U, Unterberg AW, et al. Remission of major depression under deep brain stimulation of the lateral habenula in a therapy-refractory patient. Biol Psychiatry. 2010;67:e9–11.
12. Proulx CD, Aronson S, Milivojevic D, Molina C, Loi A, Monk B, et al. A neural pathway controlling motivation to exert effort. Proc Natl Acad Sci USA. 2018;115:5792–7.
13. Krishnan V, Han M-H, Graham DL, Berton O, Renthal W, Russo SJ, et al. Molecular adaptations underlying susceptibility and resistance to social defeat in brain reward regions. Cell 2007;131:391–404.
14. Nakayama H, Abe M, Morimoto C, Iida T, Okabe S, Sakimura K, et al. Microglia permit climbing fiber elimination by promoting GABAergic inhibition in the developing cerebellum. Nat Commun. 2018;9:2830.
15. Golden SA, Covington HE, Berton O, Russo SJ. A standardized protocol for repeated social defeat stress in mice. Nat Protoc. 2011;6:1183–91.
16. Robinson MD, Oshlack A. A scaling normalization method for differential expression analysis of RNA-seq data. Genome Biol. 2010;11:R25.
17. Liao Y, Smyth GK, Shi W. featureCounts: an efficient general purpose program for assigning sequence reads to genomic features. Bioinformatics 2014;30:923–30.
18. Robinson MD, McCarthy DJ, Smyth GK. edgeR: a Bioconductor package for differential expression analysis of digital gene expression data. Bioinformatics 2010;26:139–40.
19. Gawlak M, Górkiewicz T, Gorlewicz A, Konopacki FA, Kaczmarek L, Wilczynski GM. High resolution in situ zymography reveals matrix metalloproteinase activity at glutamatergic synapses. Neuroscience 2009;158:167–76.
20. Morioka N, Abdin MJ, Kitayama T, Morita K, Nakata Y, Dohi T. P2X7 receptor stimulation in primary cultures of rat spinal microglia induces downregulation of the activity for glutamate transport. Glia 2008;56:528–38.
21. Enokido Y, Tamura T, Ito H, Arumughan A, Komuro A, Shiwaku H, et al. Mutant huntingtin impairs Ku70-mediated DNA repair. J Cell Biol. 2010;189:425–43.
22. Wohleb ES, Powell ND, Godbout JP, Sheridan JF. Stress-induced recruitment of bone marrow-derived monocytes to the brain promotes anxiety-like behavior. J Neurosci. 2013;33:13820–33.
23. Nie X, Kitaoka S, Tanaka K, Segi-Nishida E, Imoto Y, Ogawa A, et al. The innate immune receptors TLR2/4 mediate repeated social defeat stress-induced social avoidance through prefrontal microglial activation. Neuron 2018;99:464–79.
24. Yang J, Anholts J, Kolbe U, Stegehuis-Kamp JA, Claas FHJ, Eikmans M. Calcium-binding proteins S100A8 and S100A9: investigation of their immune regulatory effect in myeloid cells. Int J Mol Sci. 2018;19:1833.
25. Sorokin L. The impact of the extracellular matrix on inflammation. Nat Rev Immunol. 2010;10:712–23.
26. Bar-Or A, Nuttall RK, Duddy M, Alter A, Kim HJ, Ifergan I, et al. Analyses of all matrix metalloproteinase members in leukocytes emphasize monocytes as major inflammatory mediators in multiple sclerosis. Brain 2003;126:2738–49.
27. Benekareddy M, Mehrotra P, Kulkarni VA, Ramakrishnan P, Dias BG, Vaidya VA. Antidepressant treatments regulate matrix metalloproteinases-2 and -9 (MMP-2/MMP-9) and tissue inhibitors of the metalloproteinases (TIMPs 1-4) in the adult rat hippocampus. Synapse 2008;62:590–600.
28. Rempe RG, Hartz AMS, Bauer B. Matrix metalloproteinases in the brain and blood-brain barrier: versatile breakers and makers. J Cereb Blood Flow Metab. 2016;36:1481–507.
29. Lively S, Schlichter LC. The microglial activation state regulates migration and roles of matrix-dissolving enzymes for invasion. J Neuroinflammation. 2013;10:75.
30. Huntley GW. Synaptic circuit remodelling by matrix metalloproteinases in health and disease. Nat Rev Neurosci. 2012;13:743–57.
31. Amo R, Aizawa H, Takahoko M, Kobayashi M, Takahashi R, Aoki T, et al. Identification of the zebrafish ventral habenula as a homolog of the mammalian lateral habenula. J Neurosci. 2010;30:1566–74.
32. Quina LA, Wang S, Ng L, Turner EE. Brn3a and Nurr1 mediate a gene regulatory pathway for habenula development. J Neurosci. 2009;29:14309–22.
33. Aizawa H, Kobayashi M, Tanaka S, Fukai T, Okamoto H. Molecular characterization of the subnuclei in rat habenula. J Comp Neurol. 2012;520:4051–66.
34. Misawa H, Nakata K, Matsuura J, Nagao M, Okuda T, Haga T. Distribution of the high-affinity choline transporter in the central nervous system of the rat. Neuroscience 2001;105:87–98.
35. Seidah NG, Prat A. The biology and therapeutic targeting of the proprotein convertases. Nat Rev Drug Discov. 2012;11:367–83.
36. Remacle AG, Rozanov DV, Fugere M, Day R, Strongin AY. Furin regulates the intracellular activation and the uptake rate of cell surface-associated MT1-MMP. Oncogene 2006;25:5648–55.
37. Klein-Szanto AJ, Bassi DE. Proprotein convertase inhibition: paralyzing the cell's master switches. Biochem Pharm. 2017;140:8–15.
38. Mu D, Cambier S, Fjellbirkeland L, Baron JL, Munger JS, Kawakatsu H, et al. The integrin αvβ8 mediates epithelial homeostasis through MT1-MMP-dependent activation of TGF-β1. J Cell Biol. 2002;157:493–507.
39. Rosenberg GA. Matrix metalloproteinases in neuroinflammation. Glia 2002;39:279–91.
40. Stawowy P, Fleck E. Proprotein convertases furin and PC5: Targeting atherosclerosis and restenosis at multiple levels. J Mol Med. 2005;83:865–75.
41. Markovic DS, Vinnakota K, Chirasani S, Synowitz M, Raguet H, Stock K, et al. Gliomas induce and exploit microglial MT1-MMP expression for tumor expansion. Proc Natl Acad Sci USA. 2009;106:12530–5.
42. Ghorpade A, Persidskaia R, Suryadevara R, Che M, Liu XJ, Persidsky Y, et al. Mononuclear phagocyte differentiation, activation, and viral infection regulate matrix metalloproteinase expression: implications for human immunodeficiency virus type 1-associated dementia. J Virol. 2001;75:6572–83.
43. Woo M-S, Park J-S, Choi I-Y, Kim W-K, Kim H-S. Inhibition of MMP-3 or -9 suppresses lipopolysaccharide-induced expression of proinflammatory cytokines and iNOS in microglia. J Neurochem. 2008;106:770–80.
44. Liu S, Kimoto T, Fujita Y, Maeda T, Liu J, Tanabe-Fujimura C, et al. ATP increases the migration of microglia across the brain endothelial cell monolayer. Biosci Rep. 2016;36:e00318.
45. Kwon KJ, Shin CY, Choi MS, Ko KH, Ko HM, Cho KS, et al. ATP induced microglial cell migration through non-transcriptional activation of matrix metalloproteinase-9. Arch Pharm Res. 2010;33:257–65.
46. Kim S, Cho SH, Kim KY, Shin KY, Kim HS, Park CH, et al. α-Synuclein induces migration of BV-2 microglial cells by up-regulation of CD44 and MT1-MMP. J Neurochem. 2009;109:1483–96.
47. Karlstetter M, Lippe E, Walczak Y, Moehle C, Aslanidis A, Mirza M, et al. Curcumin is a potent modulator of microglial gene expression and migration. J Neuroinflammation. 2011;8:125.
48. Matsuda T, Sun D, Baba A, Yuan H, Ferrazzano P, Cengiz P, et al. Stimulation of Na+/H+ exchanger isoform 1 promotes microglial migration. PLoS ONE. 2013;8:e74201.
49. Yang Y, Wang H, Hu J, Hu H. Lateral habenula in the pathophysiology of depression. Curr Opin Neurobiol. 2018;48:90–6.
50. Cui Y, Yang Y, Ni Z, Dong Y, Cai G, Foncelle A, et al. Astroglial Kir4.1 in the lateral habenula drives neuronal bursts in depression. Nature 2018;554:323–7.
51. Mizoguchi H, Yamada K, Nabeshima T. Matrix metalloproteinases contribute to neuronal dysfunction in animal models of drug dependence, Alzheimer's disease, and epilepsy. Biochem Res Int. 2011;2011:1–10.
52. Verslegers M, Lemmens K, Van Hove I, Moons L. Matrix metalloproteinase-2 and -9 as promising benefactors in development, plasticity and repair of the nervous system. Prog Neurobiol. 2013;105:60–78.
53. Shibasaki C, Takebayashi M, Itagaki K, Abe H, Kajitani N, Okada-Tsuchioka M, et al. Altered serum levels of matrix metalloproteinase-2, -9 in response to electroconvulsive therapy for mood disorders. Int J Neuropsychopharmacol. 2016;19:pyw019.
54. Shibasaki C, Itagaki K, Abe H, Kajitani N, Okada-Tsuchioka M, Takebayashi M. Possible association between serum matrix metalloproteinase-9 (MMP-9) levels and relapse in depressed patients following electroconvulsive therapy (ECT). Int J Neuropsychopharmacol. 2018;21:236–41.

55. Artenstein AW, Opal SM. Proprotein convertases in health and disease. New Engl J Med. 2011;365:2507–18.
56. Cain BM, Vishnuvardhan D, Wang W, Foulon T, Cadel S, Cohen P, et al. Production, purification, and characterization of recombinant prohormone convertase 5 from baculovirus-infected insect cells. Protein Expr Purif. 2002;24:227–33.
57. Bassi DE, Fu J, De Cicco RL, Klein-Szanto AJP. Proprotein convertases: 'Master switches' in the regulation of tumor growth and progression. Mol Carcinog. 2005;44:151–61.
58. Tombácz D, Maróti Z, Kalmár T, Csabai Z, Balázs Z, Takahashi S, et al. High-coverage whole-exome sequencing identifies candidate genes for suicide in victims with major depressive disorder. Sci Rep. 2017;7:7106.